AFRL-AFOSR-VA-TR-2019-0209

A Multi-Physics Approach to Validation of Failure Models in Extreme Thermoacoustic Environments

John Lambros
UNIVERSITY OF ILLINOIS

03/06/2019
Final Report

Air Force Research Laboratory
AF Office Of Scientific Research (AFOSR)/ RTA1
Arlington, Virginia 22203
Air Force Materiel Command

REPORT DOCUMENTATION PAGE

Form Approved
OMB No. 0704-0188

1. REPORT DATE *(DD-MM-YYYY)*	2. REPORT TYPE	3. DATES COVERED *(From - To)*
24-07-2019	Final Performance	01 Dec 2015 to 30 Nov 2018

4. TITLE AND SUBTITLE
A Multi-Physics Approach to Validation of Failure Models in Extreme Thermoacoustic Environments

5a. CONTRACT NUMBER

5b. GRANT NUMBER
FA9550-16-1-0055

5c. PROGRAM ELEMENT NUMBER
61102F

6. AUTHOR(S)
John Lambros

5d. PROJECT NUMBER

5e. TASK NUMBER

5f. WORK UNIT NUMBER

7. PERFORMING ORGANIZATION NAME(S) AND ADDRESS(ES)
UNIVERSITY OF ILLINOIS
506 S WRIGHT STREET SUITE 364
URBANA, IL 61801-3649 US

8. PERFORMING ORGANIZATION REPORT NUMBER

9. SPONSORING/MONITORING AGENCY NAME(S) AND ADDRESS(ES)
AF Office of Scientific Research
875 N. Randolph St. Room 3112
Arlington, VA 22203

10. SPONSOR/MONITOR'S ACRONYM(S)
AFRL/AFOSR RTA1

11. SPONSOR/MONITOR'S REPORT NUMBER(S)
AFRL-AFOSR-VA-TR-2019-0209

12. DISTRIBUTION/AVAILABILITY STATEMENT
A DISTRIBUTION UNLIMITED: PB Public Release

13. SUPPLEMENTARY NOTES

14. ABSTRACT

Failure of thin aerospace panels in the hypersonic environment has posed as a complex problem to researchers and vehicle designers in recent decades. Prior work has highlighted the complicated resonant behavior of simple structures in a combined loading environment of vibration and heating. The effects of various heating distributions on pre-thermally buckled and post-thermally buckled plates have been evaluated in theoretical and experimental work. Fatigue failure caused by in-plane thermal gradients from localized heating, vibration, and mechanical boundary conditions has not been well addressed in the laboratory setting. The present work adds to current understanding of this topic with a series of experiments which investigate structural response and failure at multiple length scales. Thin aerospace-type beams and plates made of a nickel super-alloy, Hastelloy X, and of Al 1100-H14 were subjected to forced vibration initially at room temperature and subsequently with localized heating to examine the effects of thermal stress gradients on structural response. Coarse-grained specimens were then produced by annealing aluminum Al 1100-O (commercially pure Al) to explore the role of microstructural phenomena in the thermoacoustic environment and their influences on global behavior. Using oligocrystal samples in this fashion made the grain scale effects occur at the same scale as the sample size and thus both effects could be investigated simultaneously. The microstructural heterogeneity of coarse-grained beams was shown to have significant effect on plastic hinging behavior at the beam root. Finally, fatigue experiments were performed in a combined loading environment to assess behavior beyond the linear elastic regime and promote plasticity and failure. Although fatigue failure was suppressed in thin beams and panels, adding a stress concentrator, such as a notch near

15. SUBJECT TERMS
thermoacoustic, fatigue, failure prediction, digital image correlation

16. SECURITY CLASSIFICATION OF:			17. LIMITATION OF ABSTRACT	18. NUMBER OF PAGES	19a. NAME OF RESPONSIBLE PERSON
a. REPORT	b. ABSTRACT	c. THIS PAGE			TILEY, JAIMIE
Unclassified	Unclassified	Unclassified	UU		19b. TELEPHONE NUMBER *(Include area code)* 703-588-8316

FINAL PROGRESS REPORT

To: structural.mech@us.af.mil
Subject: Final year report to Dr. Jaimie S. Tiley, AFOSR/RTA1

Contract/Grant Title: A Multi-Physics Approach to Validation of Failure Models in Extreme Thermoacoustic Environments
Contract/Grant #: FA9550-16-1-0055
Reporting Period: 1 December 2015 to 30 November 2018

Abstract (more than 250 words):

Failure of thin aerospace panels in the hypersonic environment has posed as a complex problem to researchers and vehicle designers in recent decades. Prior work has highlighted the complicated resonant behavior of simple structures in a combined loading environment of vibration and heating. The effects of various heating distributions on pre-thermally buckled and post-thermally buckled plates have been evaluated in theoretical and experimental work. Fatigue failure caused by in-plane thermal gradients from localized heating, vibration, and mechanical boundary conditions has not been well addressed in the laboratory setting. The present work adds to current understanding of this topic with a series of experiments which investigate structural response and failure at multiple length scales. Thin aerospace-type beams and plates made of a nickel super-alloy, Hastelloy X, and of Al 1100-H14 were subjected to forced vibration initially at room temperature and subsequently with localized heating to examine the effects of thermal stress gradients on structural response. Coarse-grained specimens were then produced by annealing aluminum Al 1100-O (commercially pure Al) to explore the role of microstructural phenomena in the thermoacoustic environment and their influences on global behavior. Using oligocrystal samples in this fashion made the grain scale effects occur at the same scale as the sample size and thus both effects could be investigated simultaneously. The microstructural heterogeneity of coarse-grained beams was shown to have significant effect on plastic hinging behavior at the beam root. Finally, fatigue experiments were performed in a combined loading environment to assess behavior beyond the linear elastic regime and promote plasticity and failure. Although fatigue failure was suppressed in thin beams and panels, adding a stress concentrator, such as a notch near the beam root, promoted fatigue crack nucleation.

1. INTRODUCTION

The pursuit of sustained hypersonic flight has presented researchers and engineers with demanding structural challenges not the least of which is structures that can survive an extreme thermoacoustic loading environment. In our context, thermoacoustic is defined as an environment in which transient or harmonic mechanical loading in the acoustic frequency range (100s to 1,000s of Hz) coexists with elevated temperature loading (100°s to 1,500°C). Laboratory basic and applied research as well as X-plane test flights provided a wealth of data on surviving vibration at high speeds and tolerating thermal stresses from intense heat. Nonetheless, the design of hypersonic flight structures was, and to a certain extent remains, an empirical process generally leading to overly conservative structural designs. Over the years, researchers have sought to further and more precisely characterize both structural and material behavior, including failure, in the extreme hypersonic flight environment in efforts to create more efficient, and ultimately effective, high-speed vehicles. The present work seeks to bridge these knowledge gaps even further by concentrating on multiscale characterization of both thermoacoustic structural response and material fatigue failure.

This study is part of a joint effort between the University of Illinois and the University of Liverpool, the latter under the auspices of a separate grant from EOARD, to develop a framework for validating fatigue failure theories in a multi-physics environment. The aspects of this work that were performed at the University of Illinois at Urbana Champaign (UIUC) are discussed in this report. Specifically, the goals of this work were to:

(a) Understand Combined Environment Structural Response: The first objective was to develop an understanding of structural response in a combined environment of high-frequency vibration and thermal loading representative of the hypersonic flight environment. In particular, the effects of localized heating, as opposed to uniform heating, and in-plane thermal gradients on vibration response were studied. In-plane stresses caused by extreme thermal gradients influence out-of-plane deflection and resonant behavior. The presented effort collected and analyzed validation-quality full-field data of this response. The addition of mechanical constraints was also an important facet of the work. The boundaries of real aerospace structures induce complex changes to structural response and can cause coupled responses in combined loading scenarios.

(b) Understand the Influence of Microstructure on Thermoacoustic Deformation: The second objective of the presented work was to investigate the role of microstructural effects in the context of combined environment loading. Mechanical behavior at the microscale governs initiation of fatigue damage as microstructural anisotropy leads to strain heterogeneity. Prior research of structures in the hypersonic environment have largely focused on global response in the presence of vibration and heating. With the addition of localized heating, the interaction between thermal gradients and microstructural features, such as grain boundaries, was an important research direction.

(c) Promote and Study Plasticity and Fatigue Failure in a Thermoacoustic Environment: Inducing plasticity and fatigue, beyond an elastic design state, are essential in understanding failure during combined loading. Again, the role of localized heating and thermal gradients was of key interest. Characterizing the effects of highly non-uniform heating on fatigue failure is crucial in studying the degradation of hypersonic vehicle structures.

2. EXPERIMENTAL METHODS

Materials: Following prior thermoacoustic and fatigue studies of our group [1-5], Hastelloy X, a nickel-based superalloy manufactured by Haynes International, was used in vibration and heating experiments. Hastelloy X sheet of 0.5 mm thickness was used to make plate and beam specimens (at 538˚C, it has a yield strength and tensile strength of 253 MPa and 628 MPa). A small thickness was selected to best match the behavior of thin aerospace panels and to more easily promote thermoacoustic fatigue failure. A second material, Aluminum 6061-T6, was also used for fatigue failure experiments due to its yield strength and fracture toughness being considerably lower than Hastelloy X. These lower properties permitted a plastic response and failure to be readily achieved during high-cycle fatigue experiments. A common aerospace alloy, Al 6061 offers relatively high strength with low density [6]. The T6 temper of Al 6061 exhibits a yield strength of 255 MPa and an ultimate tensile strength of 290 MPa at room temperature. Al 6061-T6 sheet of 0.4 mm thickness was used to make plate and beam specimens. Finally, Aluminum 1100, otherwise known as commercially pure aluminum, was used to make coarse-grained specimens for experiments studying influence of microstructure on global response. Al 1100 was selected because of the ease of growing its grains with moderate heat treatment. The 99% aluminum content of Al 1100 allows for significant grain growth during annealing, which led to beams and plates with millimeter-sized recrystallized regions. These specimens, known as oligocrystals, are characterized by grains with sizes comparable to the length scale of the entire specimen. Oligocrystals have fewer grains than a representative volume element of the material and thus may exhibit anisotropic and heterogeneous properties. Two different tempers of Al 1100 were used in the present work due to the availability of the material at the time of purchase. Al 1100-O sheet of 1.5 mm thickness and Al 1100-H14 sheet of 0.8 mm thickness were used to make plate and beam specimens.

Specimens and loading configurations: Rectangular thin plates and beams were used for thermal loading and vibration experiments. These geometries have been studied in prior work and bear fundamental semblance to aerospace structural components, particularly thin skin panels and thin bulkheads susceptible to thermoacoustic fatigue failure. Additionally, analytical solutions of linear elastic beam and plate behavior are well known and can be used to validate simple experimental results. Cantilevered beams used to study resonant behavior were relatively large (up to 30 cm in length). The compliant nature of these specimens allowed the first several resonant modes to be observed at frequencies below 200 Hz. The large size benefitted the quality of experimental results by permitting large out-of-plane deflections during vibration loading. The experimental setup for the cantilevered beam is shown in Figure 1. Large doubly clamped beams, as seen in Figure 2, were used in initial harmonic vibration fatigue experiments with and without localized heating. Cantilevered and doubly clamped beams used to study broadband response and fatigue failure were significantly smaller than those used to survey resonant modes. Downsizing these specimens to 4.5 cm in length promoted plasticity and fatigue failure more quickly than with large specimens. This change in specimen size was crucial in probing beyond the linear elastic regime (Figure 3).

Fully fixed rectangular plate specimens were also used for thermal only loading experiments. These plates had a visible area of 5 cm x 7 cm for imaging. A border of 2 cm on each side of the plates was fixed, making the total size of each plate 9 cm x 11 cm. A steel frame, shown in Figure 4 was used to fully constrain plate specimens. A front face was connected to a

rear face and base with 16 bolts on the frame edges. The specimen was sandwiched between the two faces and the entire assembly bolted directly to the optical table. The edges of the frame were slightly beveled to achieve an unobscured view of the specimen during imaging.

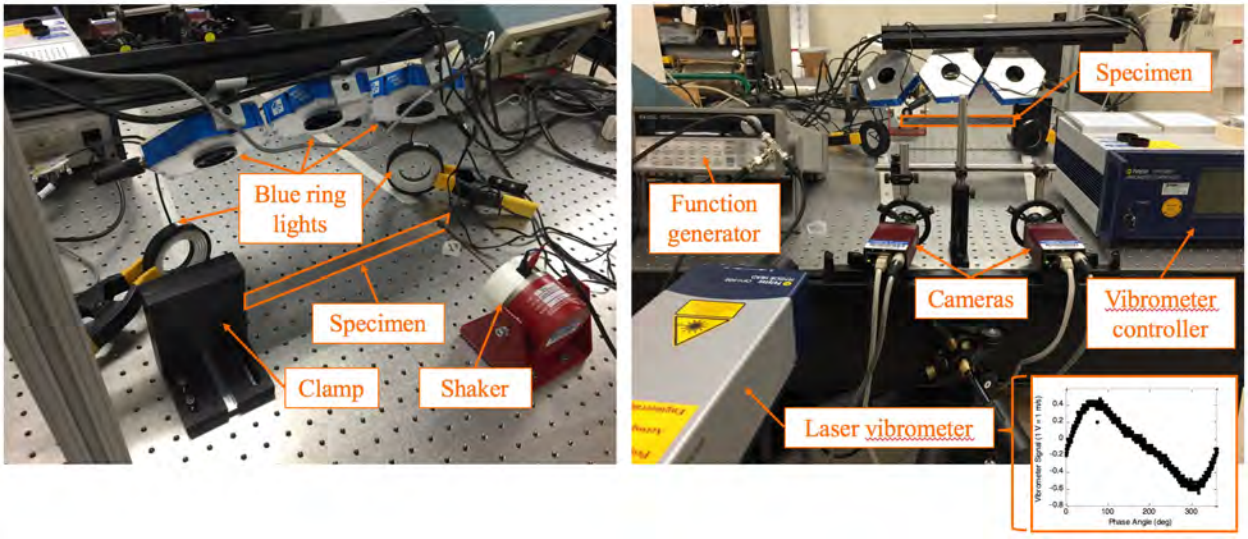

Figure 1: Cantilevered beam vibration experimental setup (front and back views).

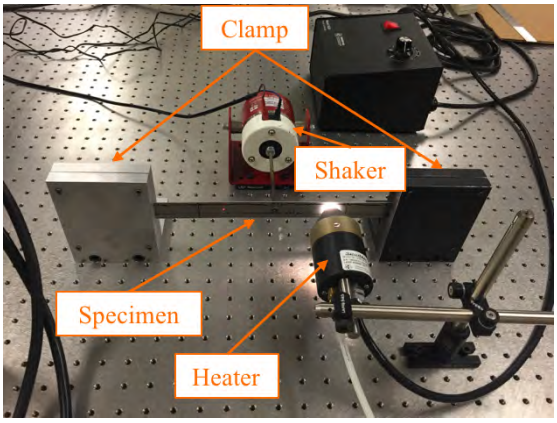

Figure 2: Large doubly clamped beam with localized heating.

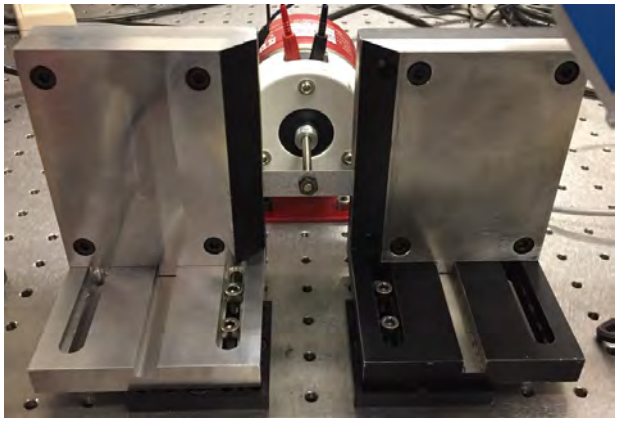

Figure 3: Small doubly clamped beam and aluminum clamps with beveled edges.

Thermal loading was provided by two OEM Heaters SpotIR heaters. Model 4085 heater used a 750-watt lamp and with a heat flux density of 101 W/cm^2 at the target surface. Model 4150 used a 250-watt lamp with a peak heat flux density of 170 W/cm^2. The heaters were mounted on optical accessory posts and brackets to be easily reconfigured to match varying arrangements of specimens and boundary conditions. These infrared heaters provided localized heating on a 0.635 cm diameter circular area with a peak temperature of 430˚C. Both heaters were fitted with air hoses to provide cooling for the infrared emitters. To further promote the localization of heating, each heater was operated with a focusing cone. These attachments enhanced the thermal gradients within specimens and thus encouraged out-of-plane deflection caused by in-plane thermal stress. A handheld FLIR TG165 microbolometer with 80 pixel x 60 pixel resolution was used to record thermal images during high temperature experiments. The

measured temperature range was limited to 380˚C, which was below the maximum heated temperature of test specimens. This range cap and the relatively low resolution of the sensor restricted use of the TG165 to establishing qualitative-only views of heating area. Because of these barriers, K-type thermocouples were also used in conjunction with the TG165 to record quantitative temperature measurements.

Vibration loading was provided by a Data Physics GW-V4 electrodynamic shaker. The maximum excitation frequency of the GW-V4 was 14 KHz. The shaker armature was connected to specimens with 7 cm-long steel threaded stinger rod. This length was short enough to mitigate rod bending during forced vibration of specimens and long enough to accommodate other experiment fixtures, such as lighting assemblies, infrared heaters, and mechanical boundary conditions. The shaker head sat on a trunnion, which was bolted directly to the optical table. The shaker was controlled in an open loop by a Hewlett Packard 33120A function generator. Harmonic vibration was used in experiments which studied the resonant behavior of cantilevered beams. Fatigue failure experiments also used harmonic loading to quantify the number of cycles until failure. Harmonic vibration, however, is not less relevant to real-world scenarios than broadband vibration. Characterizing structural response under both harmonic and broadband excitation was important in pursuing later goals of introducing localized heating and inducing plasticity and fatigue failure. The function generator supplied 10 MHz bandwidth Gaussian noise to the shaker during broadband excitation experiments. Laser Doppler Vibrometry (LDV) was used during vibration experiments to verify the frequency of excitation and identify resonant modes. A Polytec OFV-505 single point laser vibrometer head and a Polytec OFV-5000 vibrometer controller were used in the present work to measure specimens' out-of-plane velocity and displacement during forced vibration (see Figure 1).

3D (Stereo) Digital Image Correlation: 3D-DIC (or stereo-DIC) uses two cameras to simultaneously record images of a specimen [7]. Capturing images from two camera perspectives allows for calculation of an object's position in all three dimensions. 3D-DIC results in the present work were generated using Correlated Solutions VIC-3D software. Images were recorded with Correlated Solutions Vic-Snap software. Two Allied Vision Prosilica GX 1050 cameras were used to record images during experiments. They have sensor resolutions of 1024 pixels x 1024 pixels and can record at up to 112 frames per second at full resolution. The 3D-DIC setup used here is shown in Figure 1. A number of studies have demonstrated improvements to traditional DIC which extend its usability to temperatures upwards of 1,200˚C [1, 8-17]. They have addressed challenges which hamper the quality of DIC images and degrade speckle patterns. Radiation from the specimen, speckle coating oxidation, and air distortion during heating are the main hurdles to overcome when performing DIC at elevated temperatures [17]. Radiation from heating can be mitigated by illuminating the specimen with monochromatic light. Because radiation is emitted in the red and infrared regimes of the electromagnetic spectrum, blue lamps are often used to illuminate experiment setups. Blue lamps, seen in Figure 4, 5, and 6, paired with blue bandpass filters placed in front of camera lenses mitigate the glowing effect of heated specimens and thus reduce unwanted image saturation. This concept has also been extended to UV light to further lessen the impact of radiation at extreme temperatures [10, 11]. 470 nm blue ring lights and blue bandpass filters were used in the presented work. Air distortion and heat hazing can also negatively affect the quality of high temperature DIC results. Air knifes can be employed to circulate heated air and reduce unwanted image distortion. For extremely high temperatures, this problem can be addressed by conducting experiments in vacuum chambers

[17]. Heat haze was not observed during the experiments discussed in the presented work and no measures were taken to lessen its impact on experimental results.

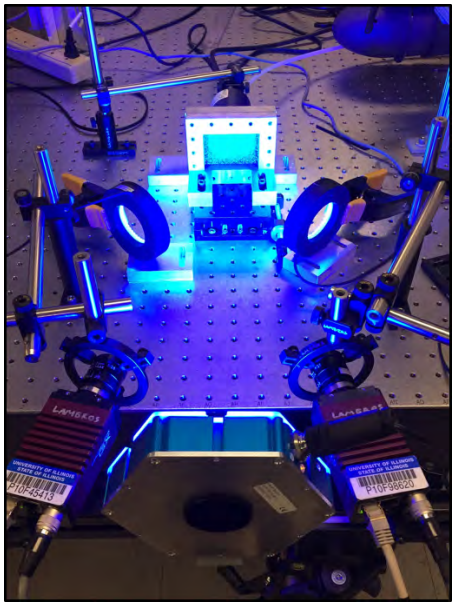

Figure 4: Fixed frame-thermal loading.

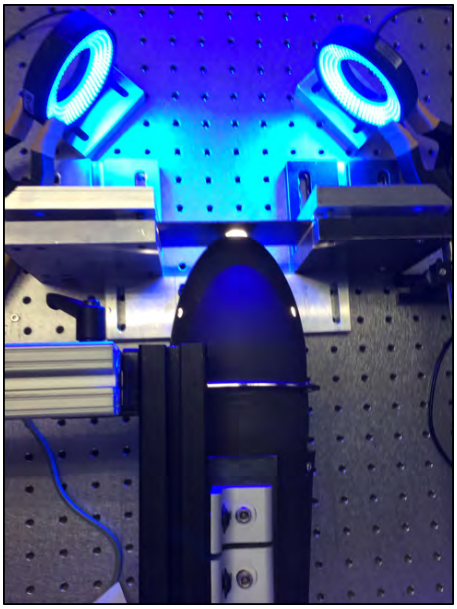

Figure 5: Doubly clamped plate-thermal loading

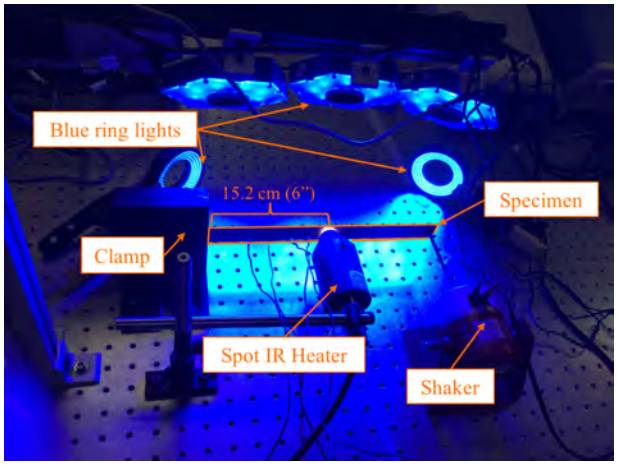

Figure 6: Blue-light DIC cantilevered beam setup with localized heating and vibration loading.

3. THERMOACOUSTIC STRUCTURAL RESPONSE

Cantilever Beam Harmonic Resonance: The resonance of a cantilevered, thin Hastelloy X beam was studied at room temperature to provide validation of our imaging techniques. Linear elastic experimental results were compared to Euler-Bernoulli beam theory to confirm that both the experimental equipment and methods were sound. The frequencies and shapes of the first four resonant modes of a cantilevered Hastelloy X beam (30 cm x 2.54 cm x 0.1 cm) were calculated before performing experiments. The experimental setup for cantilevered beam vibration is shown in Figure 1. To detect resonance conditions as loading frequency was increased, the vibrometer was directed at a non-vibration node (of non-zero displacement) location of the beam during imaging. An example of the laser vibrometer signal is included in the bottom right corner of Figure 1. DIC image sets were recorded at each of the first four resonant frequencies. The Prosilica cameras did not have high-speed imaging capabilities to record time-resolved images of the vibrating beam. A phase-stepping imaging method was used instead [1]. Figure 7 shows a VIC-3D visualization of out-of-plane displacement of the cantilevered beam's third resonant mode. In fact, the theoretical and experimental frequencies of the first four resonant modes showed very good agreement and are listed in Table 1.

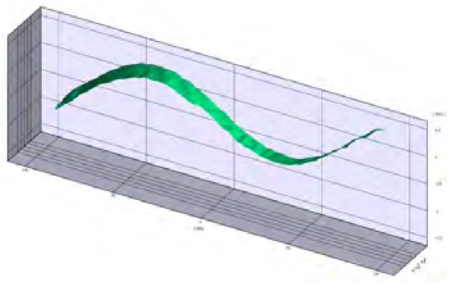

Figure 7: Mode 3 of the cantilevered beam from VIC-3D

Table 1: Theoretical and Experimental Frequencies of Cantilevered Beam Modes 1-4.

	Mode 1	**Mode 2**	**Mode 3**	**Mode 4**
Theoretical Resonant Frequency (Hz)	8.7	54.4	152.4	298.6
Experimental Resonant Frequency (Hz)	7.5	47	153	304

Broadband Loading Response: Broadband excitation experiments were performed with a doubly clamped beam but with aluminum instead of Hastelloy X. The greater compliance of the Al 6061-T6 beam compared to Hastelloy X was practically significant due to a lower shaker force during broadband excitation and stiffening caused by a second fixed boundary. A stiff Hastelloy X specimen would have likely exhibited little out-of-plane deflection and a poor signal-to-noise ratio. Phase-stepping was not applicable to the broadband excitation experiments because neither loading nor beam motion were periodic (Figure 8). To overcome motion blur, camera gain was increased, lighting was moved closer to the specimen, and exposure times were reduced to 30 μs (compared to 500 μs for harmonic excitation experiments). DIC images were captured at 50 frames per second (every 20 ms) for 5 seconds (Figure 8). Broadband excitation of the doubly clamped beam resulted in "generic" out-of-plane deflected shapes. While the transitions between these shapes were rapid, the shapes themselves were consistent in the experimental results. Figure 9 shows out-of-plane displacement of the first generic shape observed during broadband excitation. Both sides of the beam in the figure are fixed. Each frame represents a DIC image set, separated by 20 ms. The sequence of frames in Figure 9 show a symmetric bowing of the beam center, matching the behavior of the first resonant mode shape of

the doubly clamped beam. The beam quickly enters and exits this configuration within the sequence of four frames.

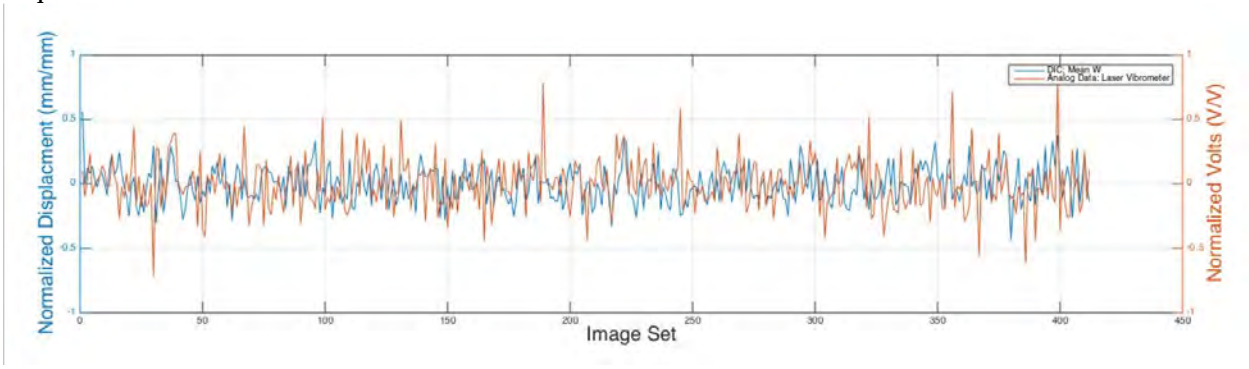

Figure 8: DIC Displacement (orange) and vibrometer measurement (blue) each normalized by its maximum value. Difference is less than 1% at all times.

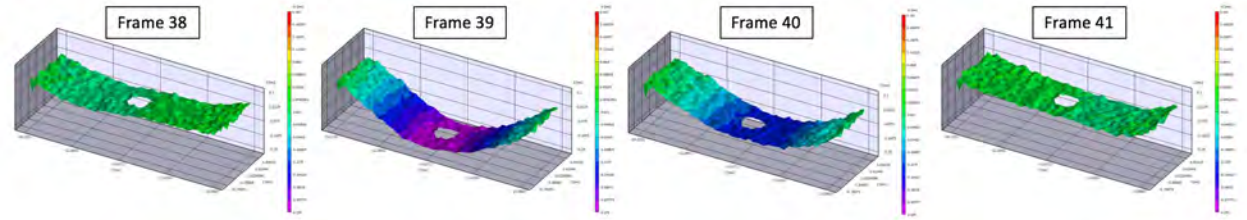

Figure 9: Doubly clamped beam mode 1 shape seen during broadband excitation.

The five-frame sequence in Figure 10 shows out-of-plane displacement of the second generic shape observed during broadband excitation. This asymmetric “S”-shape is characterized by the left and right sides of the beam deforming in opposite directions. This observed shape coincides with the second resonant mode of the doubly clamped beam. The beam predominantly occupied these two shapes resembling its first and second resonant modes.

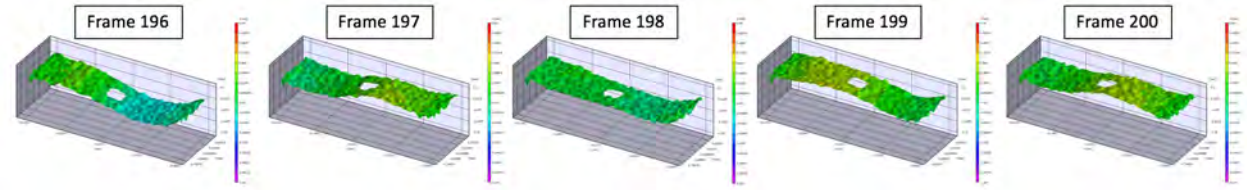

Figure 10: Doubly clamped beam mode 2 shape from broadband excitation

Thermal Loading Response–Doubly Clamped Plate: Thermal (only) loading experiments were performed on doubly clamped Al 1100 and Hastelloy X plates (7.5 cm x 8 cm) to quantify the in-plane constraint caused by localized heating. All plates were heated by the SpotIR 4150 for three minutes at 90% power and naturally cooled for seven minutes. The SpotIR was placed directly behind the center of the plates. DIC images were recorded every 10 seconds for all 10 minutes of heating and cooling. Localized heating for a 1.5 mm-thick Al-1100-O plate did not cause significant deformation (results not shown). The same localized heating procedure was performed on an Al 1100-H14 plate of 0.8 mm thickness. Figure 11 shows the out-of-plane displacement and in-plane strains at the peak of localized heating. There was significant deformation (0.8 mm) as well as increased strains at the plate center due to heating. The effect of

localized heating is evident in strain fields despite measurement noise, particularly at the contour borders. Figure 12 shows the out-of-plane shape before, during, and after heating. A clear bowing of the plate is seen in the center contour at the peak of heating as the plate center moved away from the cameras. An asymmetric residual plastic deformation is evident in the right contour where the plate center remained slightly bent.

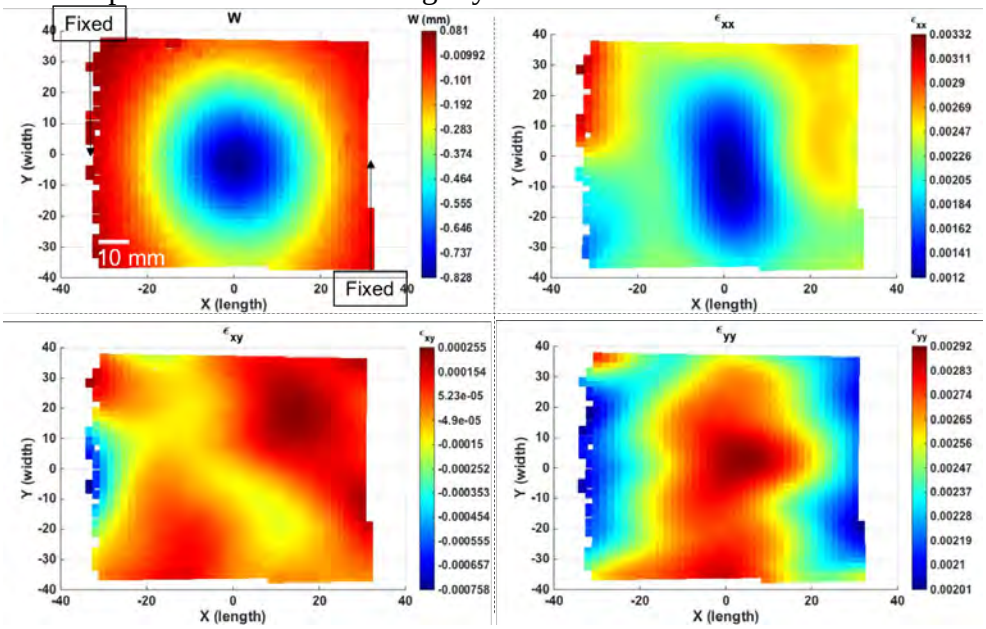

Figure 11: Out-of-plane displacement (w) and in-plane strains (ε_{xx}, ε_{xy}, ε_{yy}) for doubly clamped Al 1100-H14 plate at 3 mins of localized heating.

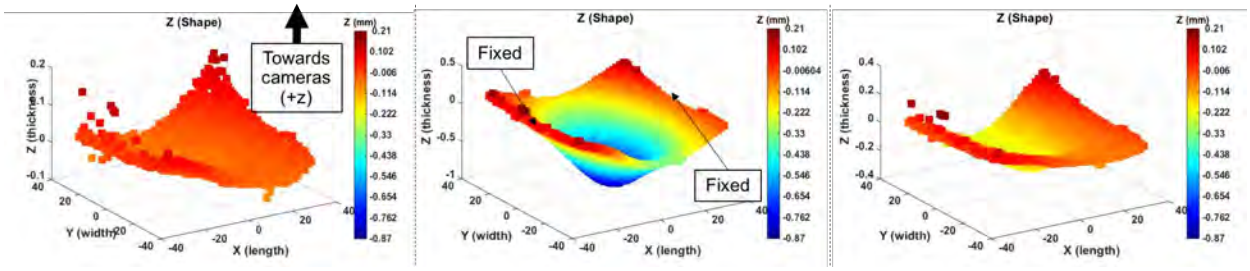

Figure 12: Out-of-plane shape (w) of the doubly clamped Al 1100-H14 plate before heating (left), at peak heating (center), and cooled (right).

A 0.5 mm-thick Hastelloy X plate was also thermally loaded with the SpotIR 4150 in the doubly clamped configuration. The Hastelloy X plate deformed more significantly than both aluminum plates, deflecting by 2.4 mm. Figure 13 shows out-of-plane displacement and in-plane strains after three minutes of localized heating. All four contours clearly display the effect of the in-plane constraint caused by heating. The greater deformation of the Hastelloy X plate than aluminum plates may be due to two main factors: thickness and thermal conductivity. The Hastelloy X specimens were the thinnest of all plates tested. The relatively high compliance from being thin may have aided in producing higher deflection when thermally loaded. The difference between the thermal conductivity of aluminum and Hastelloy X was also important factor to consider. At room temperature, pure aluminum has a thermal conductivity of 204 W/m K whereas that of Hastelloy X is only 9.2 W/m K [18-19]. The low thermal conductivity of

Hastelloy X may have increased the effect of the localized thermal load as heat was not dissipated away as effectively as in the aluminum plates. Another interesting difference between the 0.8 mm-thick aluminum and 0.5 mm-thick Hastelloy X plates was that the aluminum plate deflected towards the heater (see Figure 12) while Figure 14 shows the Hastelloy X moving away from the heater. This may have been caused by the plates' initial shapes. Figure 12 shows the aluminum plate was bent slightly towards the heater but Figure 14 displays less of an initial curvature for the Hastelloy X plate. Both exhibited a residual plastic deformation.

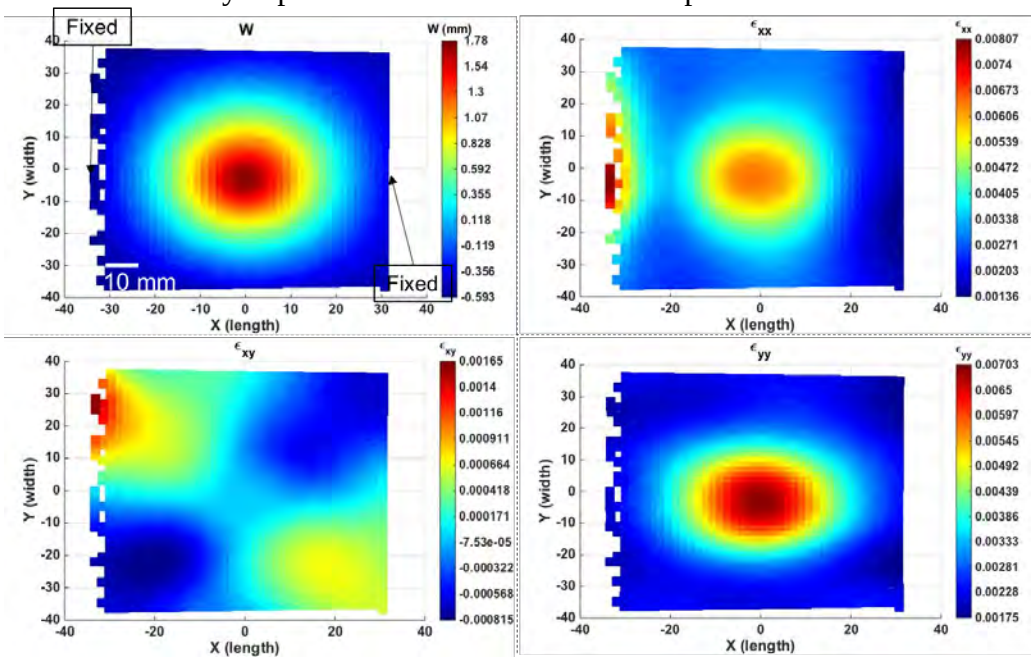

Figure 13: Out-of-plane displacement (w) and in-plane strains (ε_{xx}, ε_{xy}, ε_{yy}) for the doubly clamped Hastelloy X plate at 3 mins of localized heating.

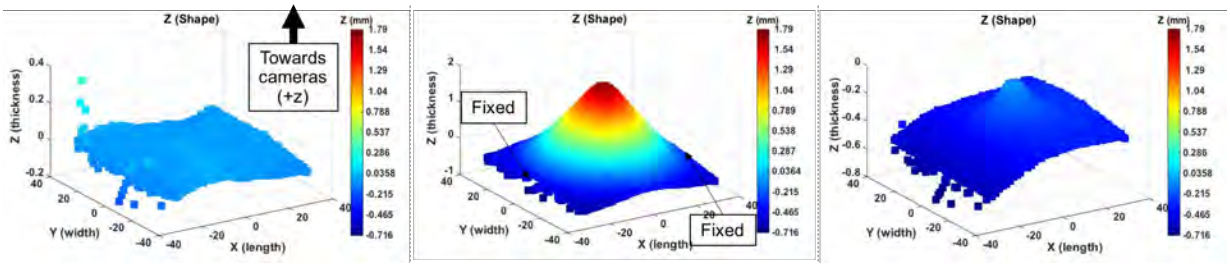

Figure 14: Out-of-plane shape (w) of the doubly clamped Hastelloy X plate before heating (left), at peak heating (center), and cooled (right)

Thermal Loading Response–All Around Fixed Plate: Fixed plates were also thermally loaded. Like the doubly clamped plates, the increased mechanical constraint (compared to cantilevered beams) and greater surface area of the plate geometry promoted a multi-axial in-plane constraint caused by localized heating. The steel fixed frame, shown in Figure 4, was used to enforce a no displacement, no slope boundary on all four sides of the plates. All fixed plates were thermally loaded with the same procedure used for the doubly clamped plates: heated for three mins at 90% power by the SpotIR 4150 and naturally cooled for seven minutes. DIC images were recorded every 10 seconds for all 10 minutes of heating and cooling. Again a 1.5

mm-thick Al 1100-O plate was loaded first. Little out-of-plane displacement was measured so a 0.8 mm-thick Al 1100-H14 fixed plate was then thermally loaded. The out-of-plane displacement and in-plane strains at peak loading are shown in Figure 15. The center of the aluminum plate deflected towards the heater by approximately 1 mm. The strain contours show a clear change from those for the 1.5 mm-thick Al 1100-O plate. The ε_{xx} and ε_{yy} fields are symmetric, with compression at the plate center and tension at the edges. As expected, tensile strain (the red contours) in the shorter y-direction (2940 με) was greater than in the longer x-direction (1680 με). Localized heating of this plate also caused a permanent residual deformation. Figure 16 shows the plate as it moved to its maximum deflection at peak heating and shows a plastic out-of-plane displacement of approximately 0.2 mm towards the heater.

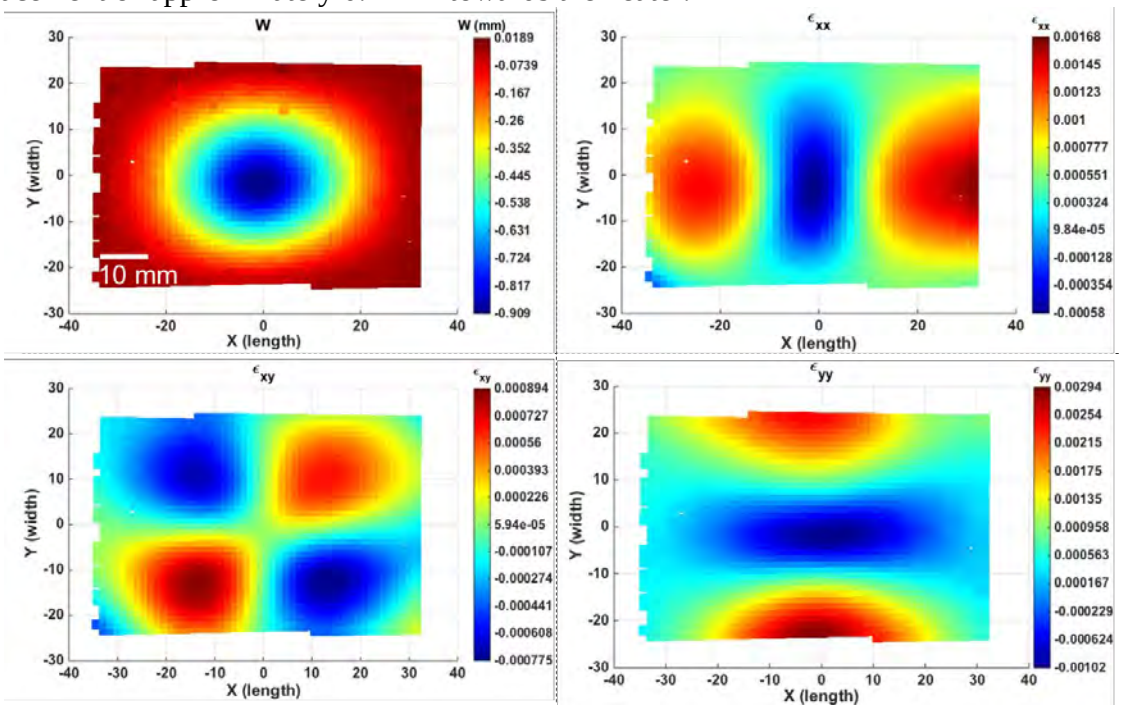

Figure 15: Out-of-plane displacement (w) and in-plane strains (ε_{xx}, ε_{xy}, ε_{yy}) of the fixed Al 1100-H14 plate at 3 mins of localized heating.

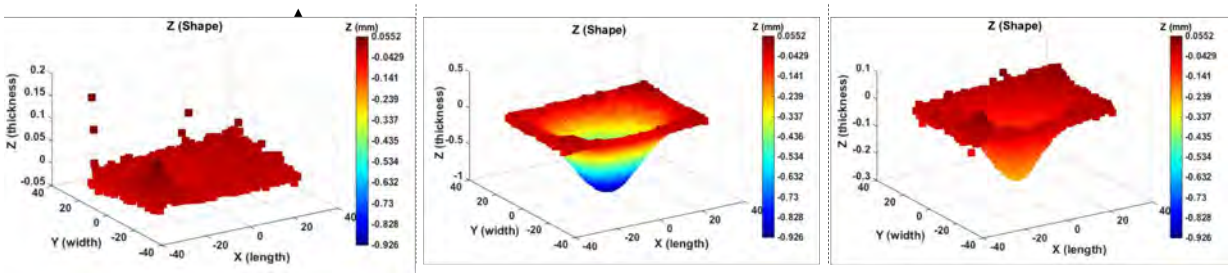

Figure 16: Out-of-plane shape (w) of the fixed Al 1100-H14 plate before heating (left), at peak heating (center), and cooled (right).

A 0.5 mm-thick Hastelloy X fixed plate was then thermally loaded in the same manner as the aluminum plates. The out-of-plane displacement and in-plane strains at peak heating are shown in Figure 17. The plate moved towards the heater, just as the Al 1100-H14 plate did. The

ε_{xx} strain field shows two maxima of strain, directly to the left and right of the plate center. The ε_{yy} contours display a saddle-like distribution of strain with tension above and below the plate center and slight compression to the left and right. The out-of-plane shapes throughout the experiments, seen in Figure 18, were similar in form. The plate was left with a residual out-of-plane displacement after cooling. As in the case of the doubly clamped plates, the thinner and less thermally conductive Hastelloy X fixed plates deformed more than the pure aluminum plates.

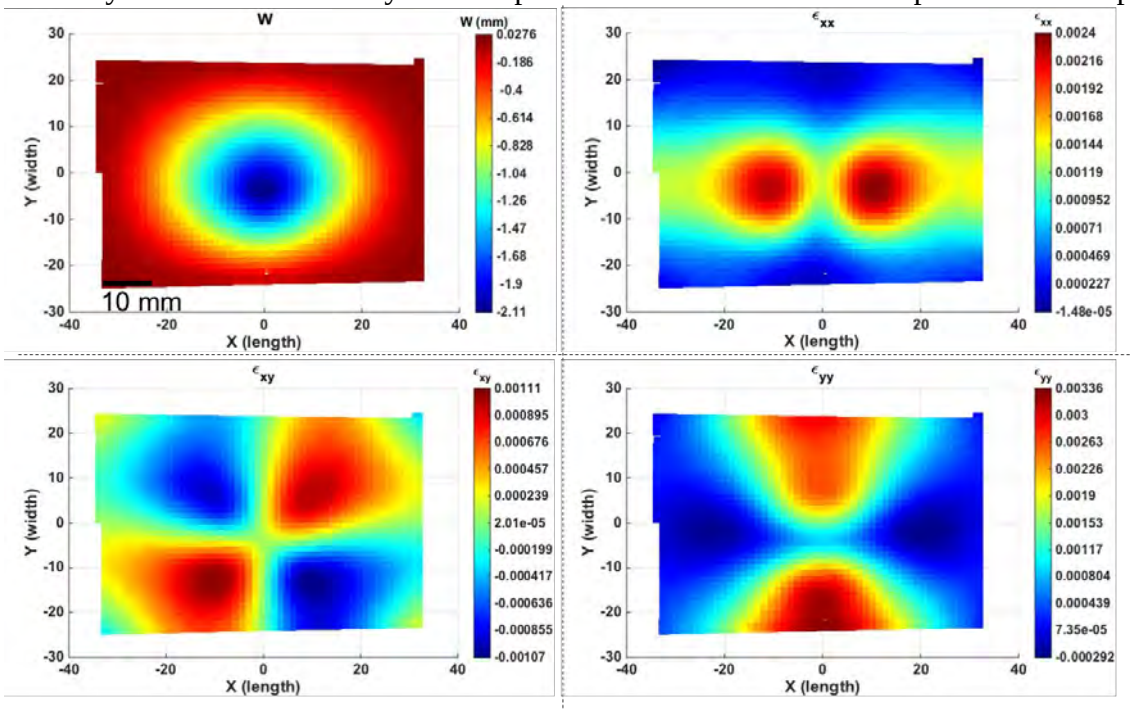

Figure 17: Out-of-plane displacement (w) and in-plane strains (ε_{xx}, ε_{xy}, ε_{yy}) of the fixed Hastelloy X plates at 3 mins of localized heating.

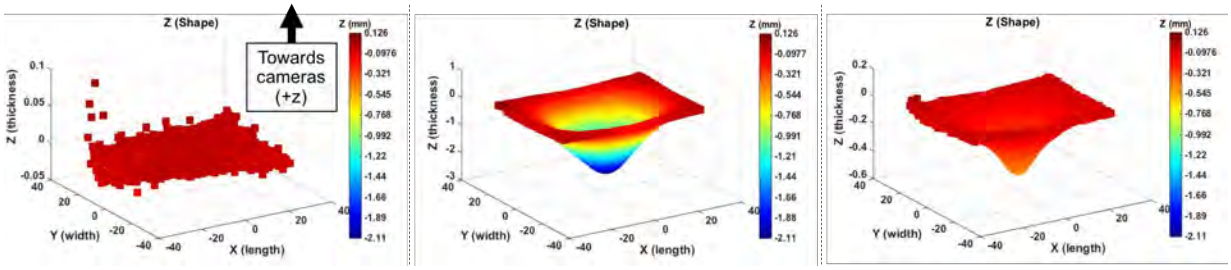

Figure 18: Out-of-plane shape (w) of the fixed Al 1100-H14 plate before heating (left), at peak heating (center), and cooled (right).

Combined Loading Response: Localized heating experiments demonstrated the effects of thermal gradients on plates with doubly clamped and fully fixed boundary conditions. In the pursuit of understanding the combined loading environment of vibration and localized thermal loads, a set of experiments were performed on a Hastelloy X cantilevered beam. The beam was forced with harmonic loading and the SpotIR 4150 was placed directly at the beam center, as shown in Figure 6. The beam was heated to a steady state and the resonant modes of the beam were identified with the same method as described above. The resonant frequency results

between the room temperature and localized heating experiments are shown in Table 2. Except for the first resonant mode, the frequency of each mode increased with the addition of localized heating. While the beam center became more compliant due to localized heating, the increase in resonant frequencies with heating suggests that the stiffness of the entire vibrating structure increased. This stiffening from localized thermal loading contrasts prior work which reported softening behavior with uniform heating [1].

Table 2: Resonant Frequencies of Cantilevered Beam Modes 1 – 4 at Room Temperature and with Localized Heating

	Mode 1	**Mode 2**	**Mode 3**	**Mode 4**
Room Temperature Frequency (Hz)	7.5	47	153	304
Localized Heating Frequency (Hz)	7.5	53	187	357

4. OLIGOCRYSTAL THERMOACOUSTIC STRUCTURAL RESPONSE

Sample preparation: The first step in this process was creating large-grained specimens through annealing of Al 1100-O. Coupon samples of Al 1100-O (1.5 cm x 1.5 cm) were placed in a Thermo Scientific™ Thermolyne™ furnace for a series of hold times at 600˚C, following the method of [20]. The grain size of the as-received aluminum was measured to be approximately 30 µm. The aluminum coupon samples were annealed for 2, 4, 6, 8, 10, 12, 24, 48, and 72 hours at 600˚C to enlarge the grains. The specimens were ground, polished, and etched to reveal grain boundaries. Figure 19 shows an aluminum beam (6.5 cm x 1.5 cm x 1.5 mm) annealed for 8 hours at 600˚C and an aluminum plate (9 cm x 11 cm x 1.5 mm) annealed for 2 hours at 600˚C. Large recrystallized regions on the right half of the beam stretch across the nearly the entire beam width while a cluster of smaller grains grew in the center region. The plate contains a mixture of grain sizes with several large centimeter-sized grains at the plate center and smaller grains interspersed throughout.

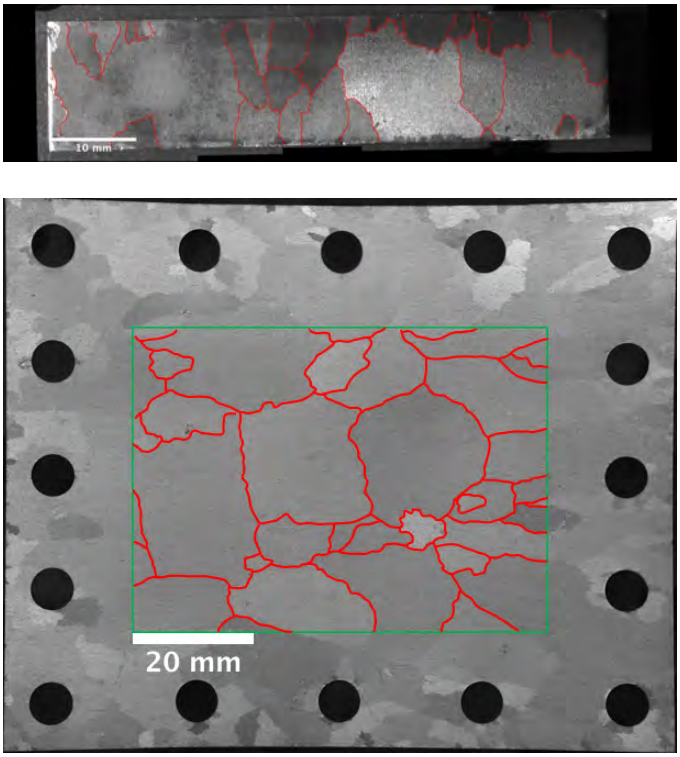

Figure 19: Al 1100-O beam annealed at 600˚C for 8 hours (top) and plate annealed at 600˚C for 2 hours (bottom) with red grain boundaries.

Beam Bend: Bending experiments were conducted with oligocrystal beams to investigate the effect of the grown grains on local and global behavior. A bending test was selected as a simplified precursor to out-of-plane vibration loading. Companion experiments were performed on beams made from as-received (i.e., fine grain) material to compare to oligocrystal experiments. The beam shown in Figure 19 was cantilevered and incrementally bent from 0 mm to 10 mm of tip displacement and 3D-DIC images were acquired at each step of bending. The residual shape of the beam after bending was also measured. Figure 20 shows axial strain fields of the beam from 1 mm to 10 mm of tip displacement. Elevated strains are clear from the

beginning of bending and become highest away from the root of the beam. This unusual behavior was compared to a beam made with as-received aluminum (Figure 21). The as-received beam displays a sharp increase in strain at the beam root, where plastic hinging occurred. This hinging at the root was not present in the oligocrystal specimen, where the heterogeneity of the oligocrystal promoted strain localization away from the root.

The oligocrystal beam bend experiments shed light on the effect of grain structure heterogeneity on out-of-plane deformation. While the response of large-grained specimens deviated clearly from the as-received specimen, no clear conclusion was drawn to link deformation to the grain structure. This may have been due to the thickness of the specimens preventing the formation of columnar large grains. Varying grain structure through the specimen thickness would have presented the impression of an oligocrystal at the surface without truly revealing oligocrystal behavior.

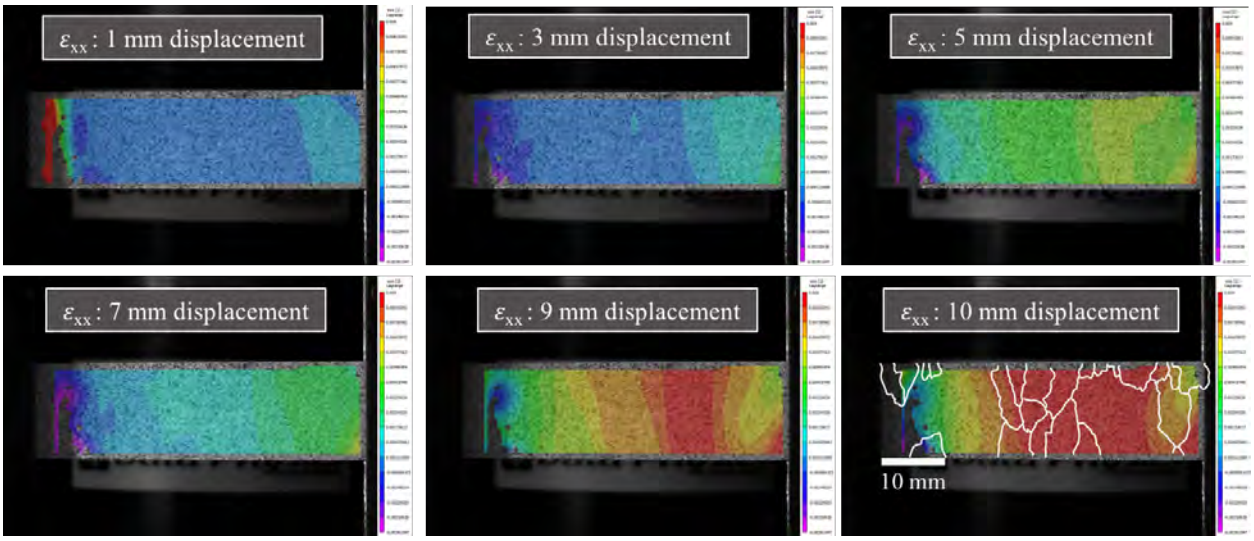

Figure 20: Axial strain fields of oligocrystal beam from 1–10 mm of tip displacement with grain map overlay.

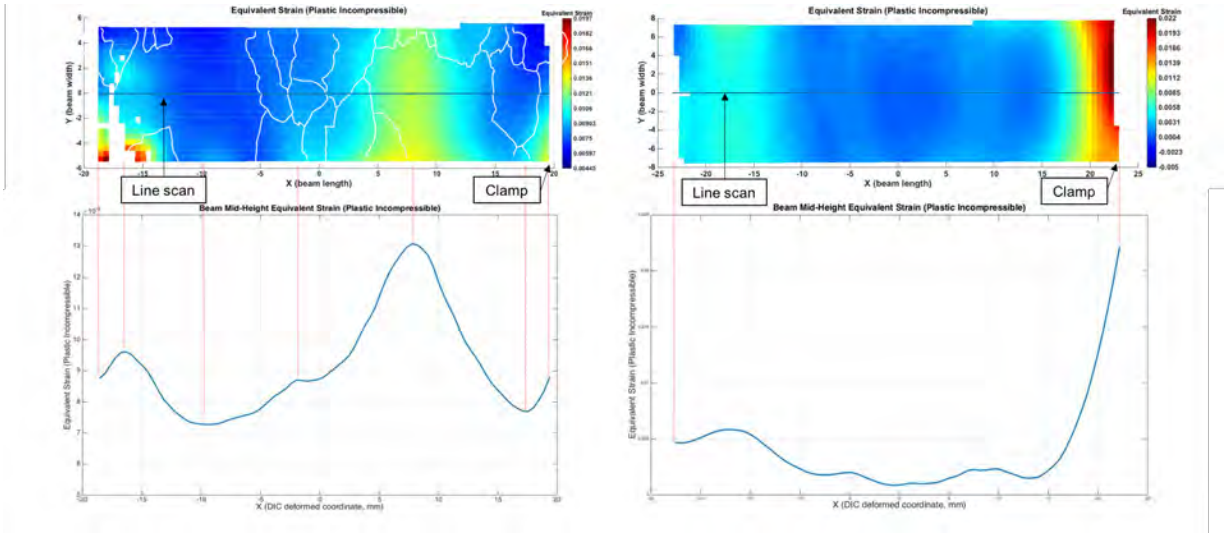

Figure 21: Residual equivalent strain in oligocrystal (left) and as-received (right) beams after 10 mm tip displacement with mid-width line scans

Plate Thermal Loading: A doubly clamped, 1.5 mm-thick Al 1100-O, annealed at 600˚C for 2 hours, was heated with the SpotIR 4150 for three minutes at 90% power and left to naturally cool for seven minutes. 3D-DIC images were recorded for all ten minutes of heating and cooling. The out-of-plane displacement and in-plane strains at peak heating are shown in Figure 22. Measurement noise can be seen in the out-of-plane displacement field. No correlation between the strain fields (color contours in Figure 22) and grain structure (white lines in Figure 22) is evident. Like the thermal loading experiments of the as-received 1.5 mm-thick aluminum plates, the large thickness and high thermal conductivity of the specimens prevented significant deformation from localized heating.

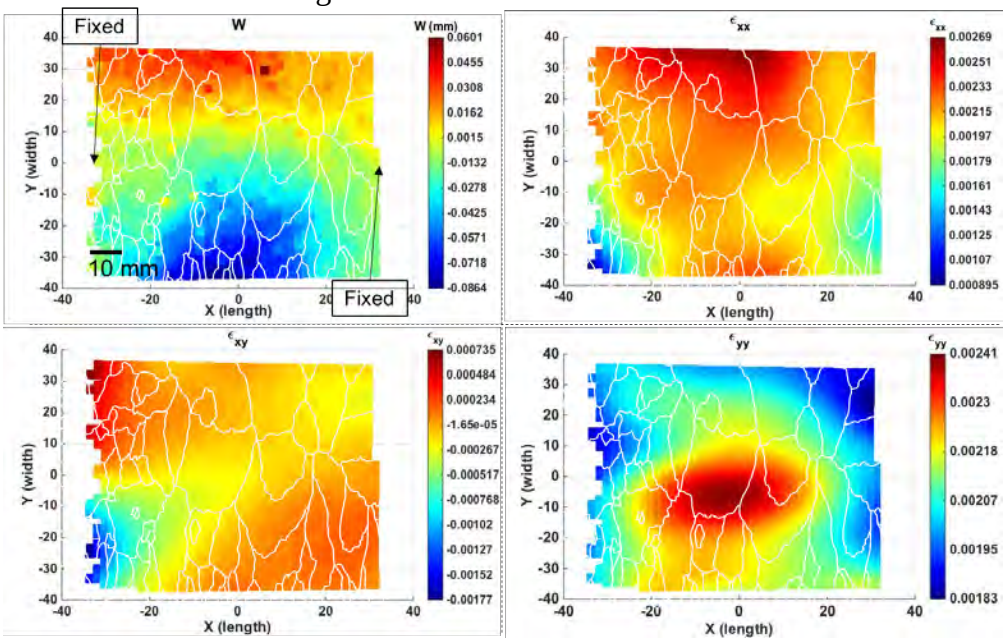

Figure 22: Out-of-plane displacement (w) and in-plane strains (ε_{xx}, ε_{xy}, ε_{yy}) of the doubly clamped Al 1100-O oligocrystal plate at 3 mins of localized heating with grain map overlay.

A fixed Al 1100-O oligocrystal plate was thermally loaded with the SpotIR 4150. The out-of-plane displacement and in-plane strains at peak heating are shown in Figure 23. The oligocrystal plate underwent greater deformation than its as-received counterpart. The plate center deflected away from the heater by approximately 0.1 mm. Tensile strains were localized at the center of heating. Some distortion is apparent in the strain fields seen in Figure 23. It was not obvious whether the asymmetry of these fields was caused by the grain structure or simply measurement noise from DIC due to small deformation. The out-of-plane shape throughout the experiment is shown in Figure 24. The plate center is seen to deform away from the heater at peak localized heating and retain a residual deformation after cooling. This was a major deviation from thermal loading response of the fixed as-received 1.5 mm-thick aluminum plate which did not experience any out-of-plane deformation. This difference highlights the likely change in bulk material properties brought about by the annealing process. While the large surface grains contributed relatively little to the response of the oligocrystal plate, the entire structure behaved differently than the untreated, as-received specimen

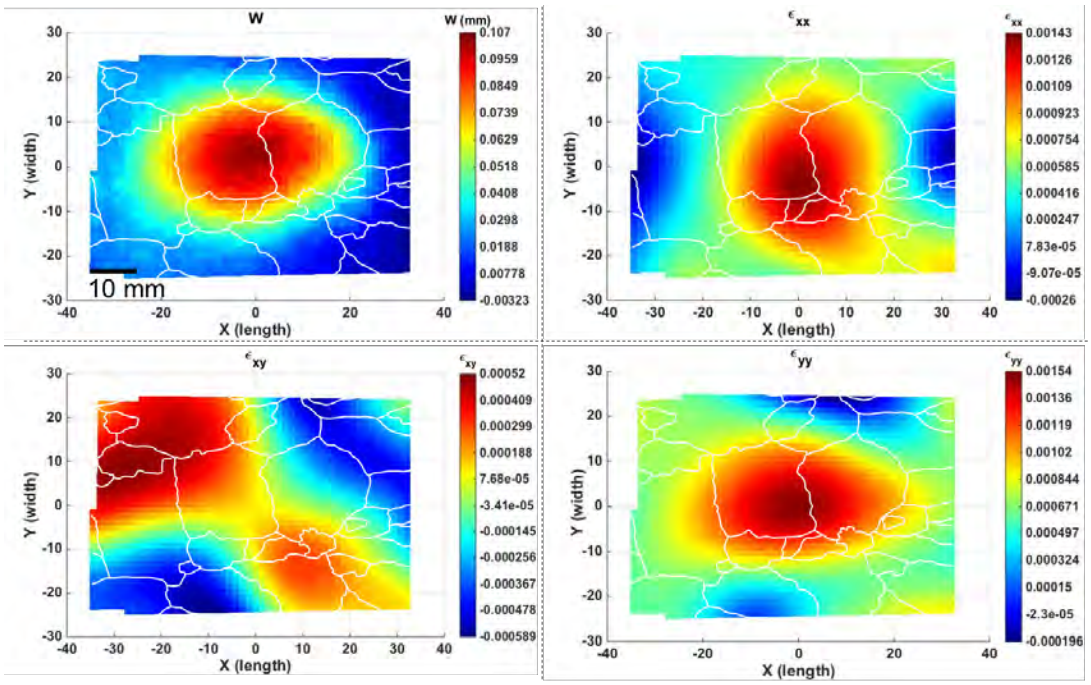

Figure 23: Out-of-plane displacement (w) and in-plane strains (ε_{xx}, ε_{xy}, ε_{yy}) of the fixed Al 1100-O oligocrystal plate at 3 mins of localized heating with grain map overlay.

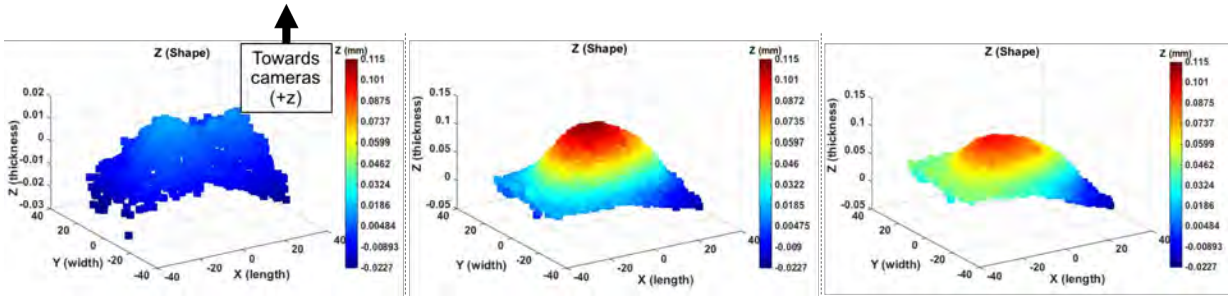

Figure 24: Out-of-plane shape (w) of the fixed Al 1100-O oligocrystal plate before heating (left), at peak heating (center), and cooled (right).

5. HIGHLIGHTS

• Studied elastic thermoacoustic structural response:

-- only small changes in natural frequencies of the structure where seen when localized heating was applied,

-- broadband loading response on average seems to consist excitation of the first or second resonant modes, although the transition between them can be abrupt,

-- significant out-of-plane deformation can occur by localized heating (even in the absence of structural loading). Local thermal gradients dictate the severity of this deformation.

• Oligocrystal thermoacoustic structural response was studied using full-field 3D DIC experimental measurements:

-- samples with large grains were grown through controlled annealing of Al,

-- although DIC-measured strain distribution did not show an immediate connection to the underlying grain structure, oligocrystal samples showed different structural responses,

-- oligocrystal cantilever beams did not form plastic hinges at their support, but rather at a large grain further away from the support (most likely the “softest” grain to stress ratio location)

-- oligocrystal plates under heating showed more asymmetry in response (likely induced by grain structure) than fine-grained as-received plates.

6. REFERENCES

[1] R. B. Berke, C. M. Sebastian, R. Chona, E. A. Patterson, and J. Lambros, “High Temperature Vibratory Response of Hastelloy-X: Stereo-DIC Measurements and Image Decomposition Analysis,” Exp. Mech., vol. 56, no. 2, pp. 231–243, 2016.

[2] M. C. Casperson, J. D. Carroll, J. Lambros, H. Sehitoglu, and R. H. Dodds, “Investigation of thermal effects on fatigue crack closure using multiscale digital image correlation experiments,” Int. J. Fatigue, vol. 61, pp. 10–20, 2014.

[3] J. Carroll, W. Abuzaid, J. Lambros, and H. Sehitoglu, “An experimental methodology to relate local strain to microstructural texture,” Rev. Sci. Instrum., vol. 81, no. 8, pp. 1–9, 2010.

[4] W. Abuzaid, A. Oral, H. Sehitoglu, J. Lambros, and H. J. Maier, “Fatigue crack initiation in Hastelloy X - The role of boundaries,” Fatigue Fract. Eng. Mater. Struct., vol. 36, no. 8, pp. 809–826, 2013.

[5] W. Abuzaid, H. Sehitoglu, and J. Lambros, “Plastic strain localization and fatigue micro-crack formation in Hastelloy X,” Mater. Sci. Eng. A, vol. 561, pp. 507–519, 2013.

[6] Alcoa, “Alloy 6061: Understanding Extruded Aluminum Alloys,” 2002.

[7] M. A. Sutton, J.-J. Orteu, and H. W. Schreier, Image Correlation for Shape, Motion and Deformation Measurements, vol. 53, no. 9. 2009.

[8] N. Cholewa, P. T. Summers, S. Feih, A. P. Mouritz, B. Y. Lattimer, and S. W. Case, “A Technique for Coupled Thermomechanical Response Measurement Using Infrared Thermography and Digital Image Correlation (TDIC),” Exp. Mech., vol. 56, pp. 145–164, 2015.

[9] B. Swaminathan, W. Abuzaid, H. Sehitoglu, and J. Lambros, “Investigation using digital image correlation of Portevin-Le Chatelier Effect in Hastelloy X under thermo-mechanical loading,” Int. J. Plast., vol. 64, pp. 177–192, 2014.

[10] R. B. Berke and J. Lambros, “Ultraviolet digital image correlation (UV-DIC) for high temperature applications,” Rev. Sci. Instrum., vol. 85, no. 4, 2014.

[11] T.Q. Thai, R.S. Hansen, A.J. Smith, J. Lambros, R.B. Berke, “Importance of Exposure Time on DIC Measurement Uncertainty at Extreme Temperatures”, accepted in Experimental Techniques, 2019.

[12] X. Chen, L. Yang, N. Xu, X. Xie, B. Sia, and R. Xu, “Cluster approach based multi-camera digital image correlation: Methodology and its application in large area high temperature measurement,” Opt. Laser Technol., vol. 57, pp. 318–326, 2014.

[13] X. Chen, N. Xu, L. Yang, and D. Xiang, “High temperature displacement and strain measurement using a monochromatic light illuminated stereo digital image correlation system,” Meas. Sci. Technol., vol. 23, no. 12, p. 125603, 2012.

[14] G. J. Pataky, H. Sehitoglu, and H. J. Maier, “High temperature fatigue crack growth of Haynes 230,” Mater. Charact., vol. 75, pp. 69–78, 2013.

[15] X. Guo, J. Liang, Z. Tang, B. Cao, and M. Yu, “High-temperature digital image correlation method for full-field deformation measurement captured with filters at 2600°C using spraying to form speckle patterns,” Opt. Eng., vol. 53, no. 6, p. 063101, 2014.

[16] M. D. Novak and F. W. Zok, “High-temperature materials testing with full-field strain measurement: Experimental design and practice,” Rev. Sci. Instrum., vol. 82, no. 11, 2011.

[17] B. M. B. Grant, H. J. Stone, P. J. Withers, and M. Preuss, “High-temperature strain field measurement using digital image correlation,” J. Strain Anal. Eng. Des., vol. 44, no. 4, pp. 263–271, 2009.

[18] Haynes International, “Hastelloy X Alloy,” 2017.
[19] Properties of Wrought Aluminum and Aluminum Alloys, vol. 2. ASM International, 1990.
[20] Z. Zhao, M. Ramesh, D. Raabe, A. M. Cuitiño, and R. Radovitzky, “Investigation of three-dimensional aspects of grain-scale plastic surface deformation of an aluminum oligocrystal,” Int. J. Plast., vol. 24, no. 12, pp. 2278–2297, 2008.